(Received 25 October 2024, Accepted 24 December 2024, Scheduled 8 January 2025)

Design of a Low-Cost Printed Slotted SIW Antenna Array with Omnidirectional Azimuth Pattern and Beam-Shaped Elevation Pattern

Tadeu P. Pasetto* and Hugo E. Hernandez-Figueroa

School of Electrical and Computer Engineering, University of Campinas, Brazil

ABSTRACT: This paper presents the design, discussions, and characterization of a low-cost printed slotted substrate integrated waveguide traveling wave antenna. The antenna exhibits an omnidirectional pattern in the azimuth plane and a cosecant squared pattern in the elevation plane. This synthesized pattern enables application in 5G mm-wave systems by providing a defined signal equipotential region, thereby increasing coverage areas in locations such as stadiums, exhibition centers, arenas, and parks. Additionally, the proposed design method facilitates the easy implementation of new designs tailored to specific installation sites.

1. INTRODUCTION

The crescent demand for data transmission driven by applications like video streaming, internet of things (IoT), and real-time communication, along with the evolution of fifth-generation cellular networks as a solution to increase wireless communication data rates, requires the development of low-cost mm-wave antennas. Also, to guarantee a desired coverage area with an equipotential signal level, it is required to design a specific radiation pattern for the antenna, with an omnidirectional pattern in azimuth cut to cover the 360° region around the antenna [1] and a cosecant squared in elevation cut [2].

Designing azimuth omnidirectional and beam-shaped pattern synthesis in the elevation cut is challenging. The typical structures used to achieve the desired amplitudes and phases for pattern synthesis, such as couplers, dividers, and delay lines [3], compromise the antenna's omnidirectionality because they act like reflectors when being placed on the antenna structure. Additionally, the most common radiant elements usually do not have an omnidirectional azimuth cut radiation pattern [4]. Furthermore, arrays are often constructed in complex ways [5], involving multiple layers of printed circuit boards (PCBs) with blind and buried vias, as well as mechanical parts [6]. This complexity demands detailed and intricate machining, making these solutions not cost-effective.

Reflector antennas with a feeder are a viable solution for meeting specific elevation radiation pattern requirements [7]. However, most commonly used feeder antennas are not omnidirectional. Also, this antenna poses challenges in their application, with the increase of the overall system complexity by requiring additional fixing points and brackets, leading to a larger antenna structure, higher costs, and potential complications in integrating the antenna with the associated microwave circuits.

Alternatively, loop antennas with scattering structures designed to modify the elevation radiation pattern can also satisfy the requirements for both azimuth and elevation coverage [8, 9]. While they present a promising solution due to their omnidirectional azimuth radiation pattern and the possibility of controlling the elevation radiation pattern, these antennas face similar challenges, including complex machined parts, high production costs, and difficulties in integration with microwave components PCB.

The traveling slotted waveguide antenna array, including traveling slotted substrate-integrated waveguide (SIW) antenna array, is a well-known type of antenna; however, regarding synthesizing its radiation pattern, some issues come about to ensure the pattern radiation requirement for more external angles. At first, the guided wavelength usually defines a distance between elements greater than a half wavelength in free space, which limits the defined synthesized region of the pattern. After that, to achieve the phase of each radiant element, there are usually two solutions, one using non-resonant uniformly spaced slots [10], defining the phase of radiation by adjusting the length of the slot, which also changes the admittance, generating an imaginary part, the amplitude of radiation, and impact at the reflection of the signal at the waveguide, and other using non-uniformly spaced resonant slots, which will work for specific cases or would present a variation to the desired pattern for more external angles without any method to synthesize the beam shape for non-uniformly spaced arrays [2, 11]. In both cases, this makes the characterization of the slots harder, considering the mutual coupling between the radiant elements concerning the length of resonance and admittance.

This paper proposes a traveling substrate integrated waveguide (SIW) antenna array operational at 28 GHz, inside the mm-

* Corresponding author: Tadeu Pasetto (tadeupasetto@gmail.com).

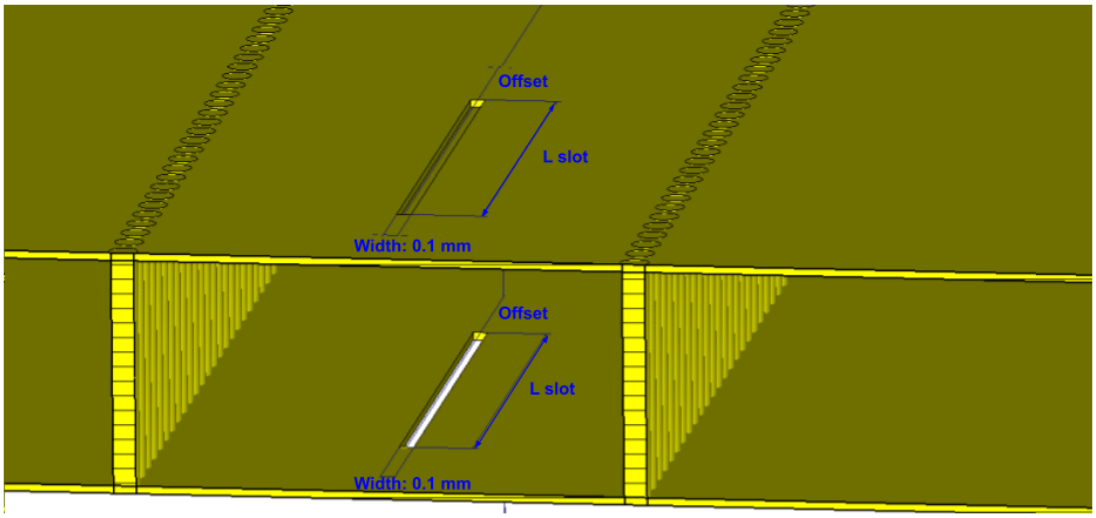

FIGURE 1. Final double slot model, without the substrate and with re-scaled axis to show the pair of slots and dimensions.

wave 5G bandwidth [2], using slots at the top and bottom layers to achieve the omnidirectional radiation pattern and nonuniform spaced elements to reach the desired radiation pattern. The antenna design procedure, preliminary presented in [12], consists of a method to synthesize the beam shape for nonuniform spaced resonant slots in a SIW. This procedure also includes the characterization of the double slots elements in the array for the length of resonance and admittance, and the analytical calculation of the antenna parameters, such as S parameters and radiation pattern. Also, this work presents the prototype construction and full characterization of the antenna, including radiation patterns in both azimuth and elevation planes and S parameters measurements.

2. SLOTTED SUBSTRATE INTEGRATED WAVEGUIDE ANTENNA

2.1. Substrate Integrated Waveguide (SIW)

SIW is a waveguide-like structure that integrates rectangular waveguides with printed microwave circuits. It uses periodic metallic vias between two conductor planes to create a rectangular waveguide equivalent structure on a PCB [13]. To avoid leakage across the periodic structure and to guarantee equivalence between the rectangular waveguide expected and the SIW, such as guided wavelength and cutoff frequency, the via diameter and the spacing between vias were calculated using [13]. The substrate used in this study was Rogers RO4350B with 20 mil thickness and a dielectric constant (ϵ_r) of 3.66 for design. The SIW at this development has a spacing between the SIW vias of 3.55 mm, equivalent to a rectangular dielectric-filled waveguide with the largest dimension of 3.4 mm to the circuital calculation [13].

2.2. Double Slot Characterization

When a slot introduces a defect in a waveguide and interrupts the current flow around the wall, generating a current around it, it radiates. In this work, the radiation element of the array is a double longitudinal slot, placed at each plane of the larger side of the waveguide and shifted from the center of the wall, which can be modeled as a shunt admittance [14]. The double slot radiating element, seen in Fig. 1 with its construction and parameters, is responsible for the omnidirectional azimuth pattern, as shown in Fig. 2.

The slot characterization is a fundamental part of the design of the array, once it guarantees the radiant amplitude and phase of each element. For a given desired design slot admittance and spacing between elements, the correspondent slot shift and length of resonance are necessary, and they should consider the mutual coupling between elements [15]. The analysis was made with 3D electromagnetic simulations at *CST Microwave Studio* with periodic boundary conditions at the waveguide propagation directions (Fig. 3), set to calculate an infinite uniformly spaced linear array with uniform amplitude of excitation and the angle of scan (Θ in Eq. (1)) defined by the phase difference caused by the spacing between the slots (d in Eq. (1)) in the waveguide (described by its guided wavelength (λ_g in Eq. (1)), given by $\Delta\phi$ in Eq. (2).

$$\Theta = \arcsin\left(\lambda_0 * \left(\frac{1}{2d} - \frac{1}{\lambda_g}\right)\right) \tag{1}$$

$$\Delta\phi = 360^\circ \times \left(\frac{d}{\lambda_g} - \frac{1}{2}\right) \tag{2}$$

The simulation was performed to find the slot resonance ($Y_{im} = 0$) by sweeping its length, considering pairs of offset from the waveguide center and spacing between slots. The results of this analysis are presented in Figs. 4 and 5. Also, the graphics show the curve fit calculation used to relate the position of the slots (or distance of slots) and desired admittance with a resonance length and an offset from the center of the waveguide.

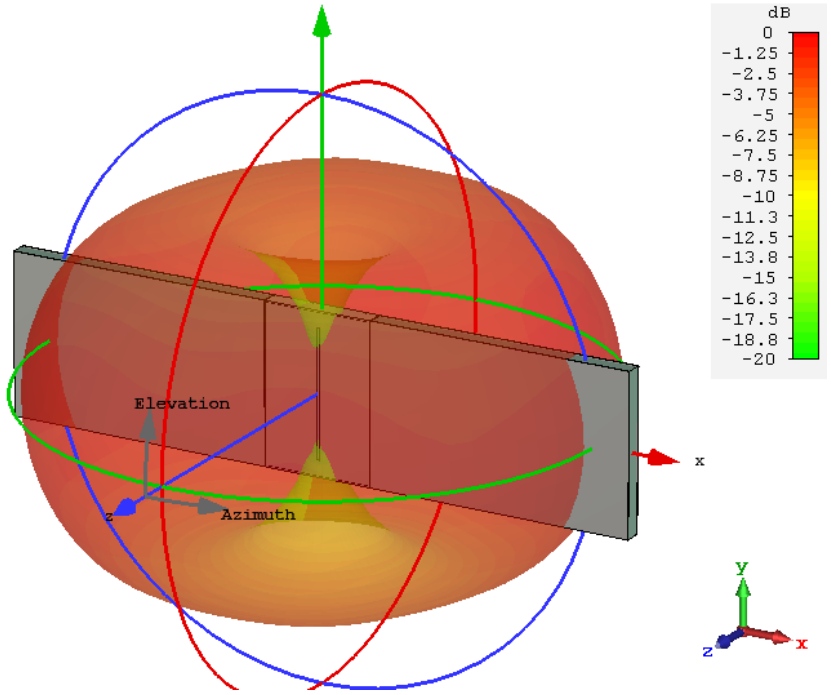

FIGURE 2. Omnidirectional radiation pattern of the 3D simulation model for the double slot with periodic boundary condition.

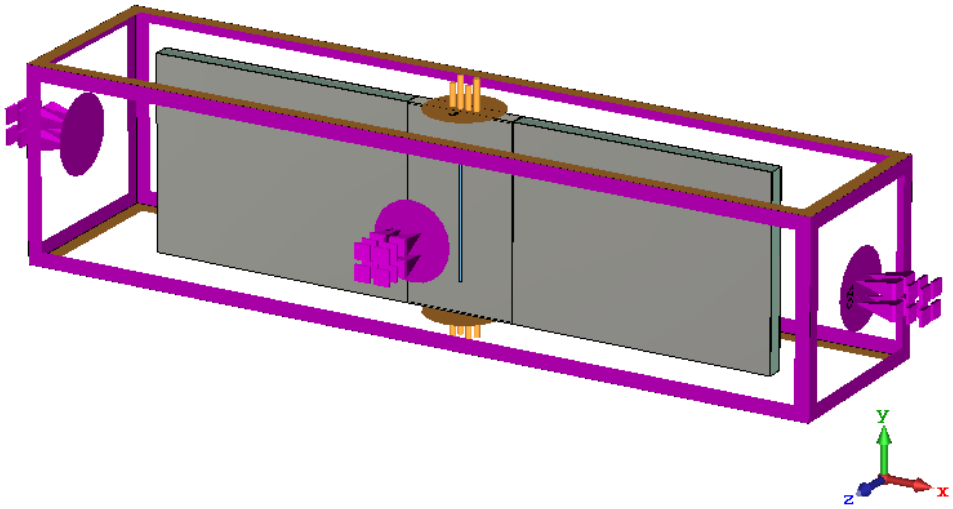

FIGURE 3. 3D simulation model for the double slot characterization using periodic boundary condition at xz plane limits.

2.3. Calculation of Radiation Pattern for a Slotted SIW Antenna

The radiation pattern for a linear array of identical elements placed along the x-axis is given by Eq. (3) [16]

$$P_{array}(\theta) = P_{el}(\theta) \sum_{i=1}^{N} \exp(j\frac{2\pi}{\lambda} x_i \sin(\theta)) a_i \qquad (3)$$

where $P_{el}(\theta)$ is the radiation pattern of the slot, which should be considered both in the analysis and synthesis of the radiation pattern; x_i is the position of the i-th element; a_i is the complex coefficient of the i-th element; and θ is the elevation angle.

Considering a generalized slotted SIW as a sequence of shunt admittances spaced by sections of a rectangular waveguide filled with dielectric, it is possible to proceed with the analytical calculation of the antenna, considering the circuit theory [17] to obtain the amplitude and phase of the signal radiated in each slot, which will represent a_i in Eq. (3), and calculate the radiation pattern of the slotted SIW antenna.

3. ARRAY RADIATION PATTERN SYNTHESIS

Writing Eq. (3) as a difference from a linear array with elements uniformly spaced of d where the i-th element is shifted of δ_i.

$$P(\theta) = P_{el}(\theta) \sum_{i=1}^{N} \exp\left(j\frac{2\pi}{\lambda} id \sin(\theta)\right)$$

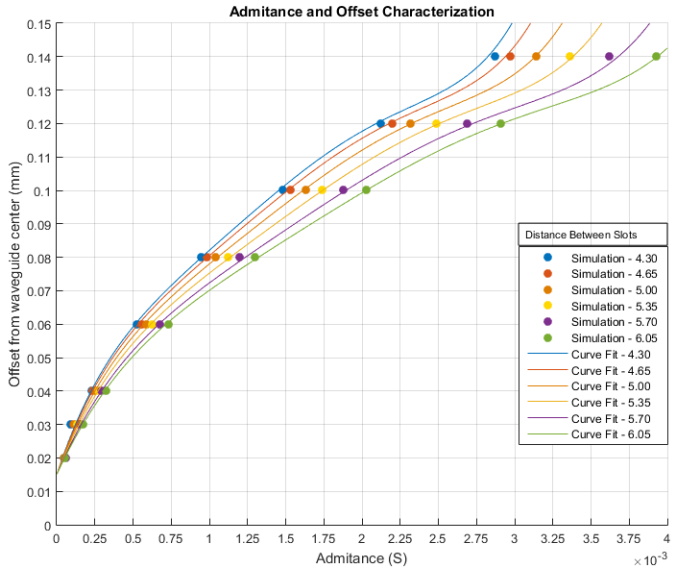

FIGURE 4. Slot characterization as function of the spacing between slots and Slot shift from waveguide center versus slot admittance.

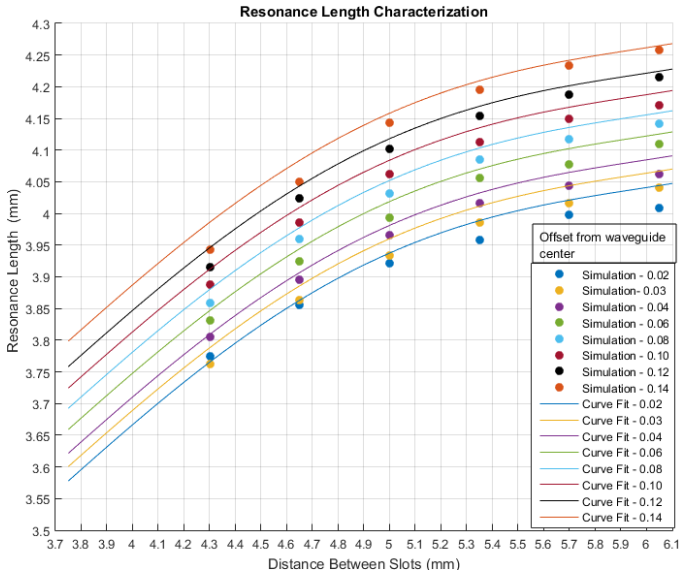

FIGURE 5. Slot characterization as function of slots spacing and slot shift versus waveguide center for Length of Resonance.

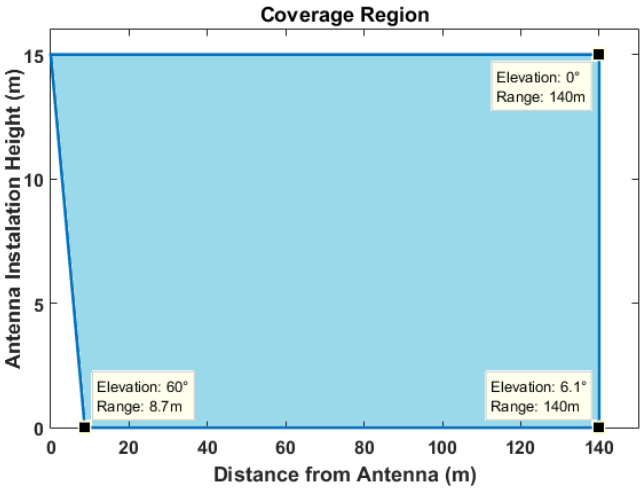

FIGURE 6. Coverage diagram for the defined radiation pattern goal.

$$\exp\left(-j\frac{2\pi}{\lambda}\delta_i \sin(\theta)\right) a_i \tag{4}$$

The term $\exp(-j\frac{2\pi}{\lambda}\delta_i \sin(\theta))$ represents an error between the uniformly and non-uniformly spaced array, and it increases for higher δ_i and also for more external θ, or higher elevations. When a_i is calculated for uniformly spaced array synthesis, this term can be neglected for small elevations, but a specific method to synthesize the coefficients for the non-uniformly spaced arrays is needed to guarantee higher elevation coverage.

This work applies a method based on the Synthesis of Shaped-Beam Radiation Patterns Using the Iterative Sampling Method [18] for non-uniformly spaced linear arrays. In each iteration, the obtained pattern is compared with the desired one, and the difference is corrected with iterative sampling.

4. DESIGN

4.1. Radiation Pattern Goal Definition

If you are planning a communication or broadcasting within an exhibition center, stadium, or any other area measuring 280 m wide (or a square of 200 × 200 m) and 15 m high, it is feasible to establish a radiation pattern that uniformly covers the periphery of this space. By positioning the antenna at the center of the arena and at a height of 15 m, the pattern needs to be omnidirectional in the azimuth cut, ensuring coverage in all directions. In the elevation cut, the pattern should commence at 0° elevation and maintain the same gain until arctan(15/140) = 6.1°, after which a $\csc^2$ pattern should be adopted from 6.1° until the desired coverage. Here, mainly due to the element radiation pattern (exhibited in Fig. 2), the $\csc^2$ was defined up to 60°, effectively covering 99.6% of the circular area. The coverage diagram, which illustrates the defined elevation radiation pattern, is presented in Fig. 6, and the $\csc^2$ here described will ensure that all the blue border of Fig. 6 will receive the same signal level from the antenna. It is important to emphasize that, owing to the omnidirectional nature of the azimuth cut, this coverage remains consistent around the antenna height axis.

4.2. Antenna Analytical Synthesis

A *Matlab* code was written to execute the calculation following the workflow described in [12]. The input parameters were the frequency of 28 GHz, the desired radiation pattern described in 4.1, the RO4350B substrate with 20 mil thickness to construct a SIW equivalent to a rectangular waveguide 3.4 mm wide, and 20 radiant elements. The outputs of the *Matlab* code include the analytical radiation pattern (shown in Fig. 7), which is compared with the goal and synthesized radiation pattern. The initial position of the slots is calculated based on a linear regression of the uniformly spaced elements coefficients phase. The position adjustment is made with the change of the slot po-

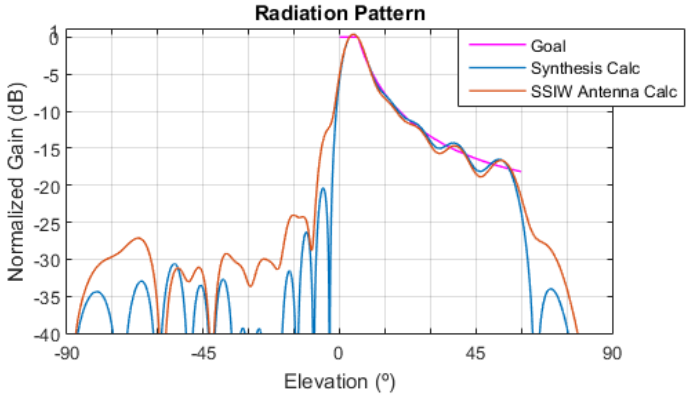

FIGURE 7. Comparison among goal, synthesized, and analytical calculation of the radiation pattern for the slotted SIW antenna.

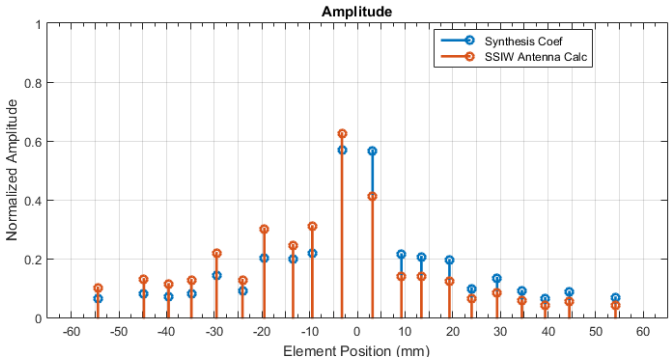

FIGURE 8. Amplitude and position of each slot for calculated synthesis coefficient and the analytical calculation for the slotted SIW antenna.

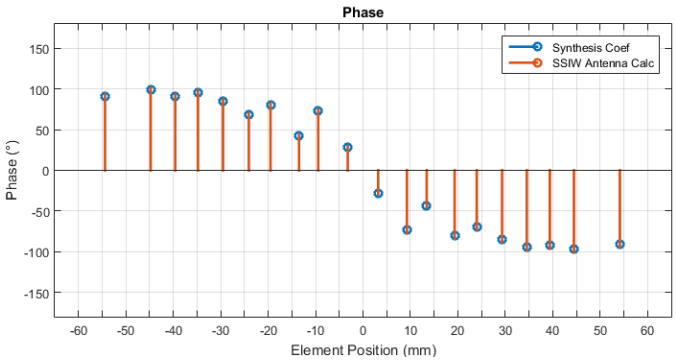

FIGURE 9. Phase and position of each slot for calculated synthesis coefficient and the analytical calculation for the slotted SIW antenna.

sition in a fraction of the guided wavelength proportional to the equivalent phase difference from the desired coefficient, always considering the possibility of inverting the direction of the shift from the center of the slot to make it radiate in the counter phase.

Additionally, the code provides S parameters for the lossless calculation, with an S_{11} of -20.3 dB and an S_{21} of -7.4 dB, indicating an efficiency of 81% due to load losses. Figs. 8 and 9 display the amplitude and phase, respectively. The position and admittance of each of the 20 slots are also given. Using these results, along with the findings from Section 2.2, it is possible to determine the length and offset from the center of the SIW for each slot and generate a 3D model for electromagnetic simulation. The results of this calculation, position, admittance, offset from the waveguide center, and length of resonance for each slot are available in Table 1.

4.3. Electromagnetic Model Simulation

A 3D model for electromagnetic simulation was developed with the outputs from the previous section and simulated in *CST Microwave Studio*. The radiation pattern result is presented in Fig. 10 as initial simulation. A particle swarm optimization of the 3D model was performed in *CST Microwave Studio* to improve the secondary lobe level (SLL). This optimization adjusted the lengths of the critical slots (Slots 1, 2, 8, 9, 10, 11, 12, 13, 19, and 20 in Table 1). The selected slots were the border slots, those with the largest distance differences from adjacent slots, and those with the greatest amplitude differences between neighboring slots based on Fig. 8. The length of the critical slots was chosen for optimization based on the variations of length in function of the distance between slots and the offset from the waveguide center shown in Fig. 5, which in some cases achieve 10% and the impacts of non-resonant slots on amplitude and phase.

Additionally, the synthesis reduced the number of variables to optimize from 60 (position, offset, and length of each of the 20 slots) to 10. The goals were to keep the SLL as low as 20 dB and the error from the analytical radiation pattern in the $\csc^2$ region below 3 dB. The optimization results are shown in Fig. 10 as optimized simulation, with the final lengths of the critical slots detailed in Table 1 and 3D radiation pattern in Fig. 11.

The effective bandwidth of the proposed antenna is defined by the tolerable variation in the radiation pattern with frequency changes, including the gain variation impacted by the power dissipated in the load. This variation is presented in Fig. 12 for elevation cut and in Fig. 13 for azimuth cut, considering 1 GHz bandwidth between 27.4 and 28.4 GHz. The results for the optimized simulation model at 28 GHz present a maximum gain of 6.8 dB and 6.4 dB in 0° azimuth cut and an efficiency of 82.2% due to load losses. The S parameters for this model are available in Fig. 14.

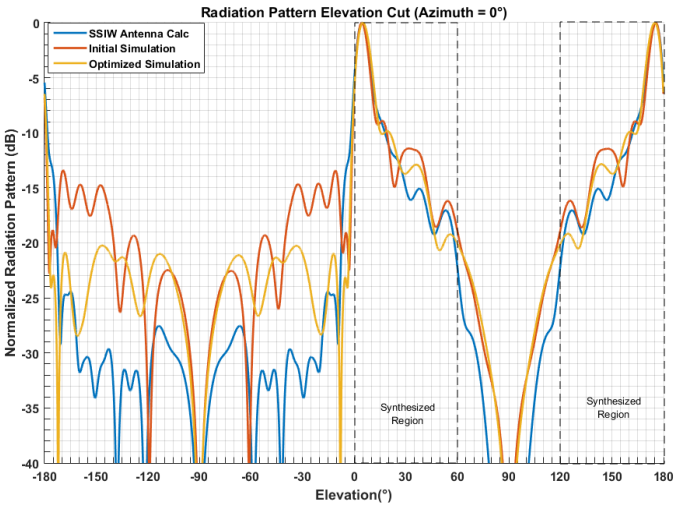

FIGURE 10. Comparison between normalized radiation pattern at elevation cut for the Analytical Calculation, Initial, and Optimized 3D simulation results.

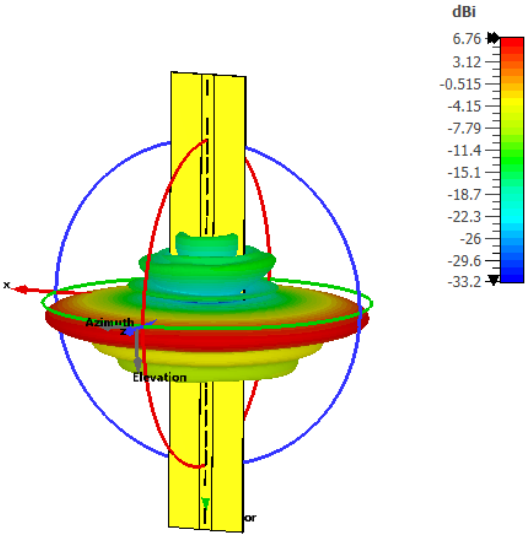

FIGURE 11. 3D simulated radiation pattern for the optimized model.

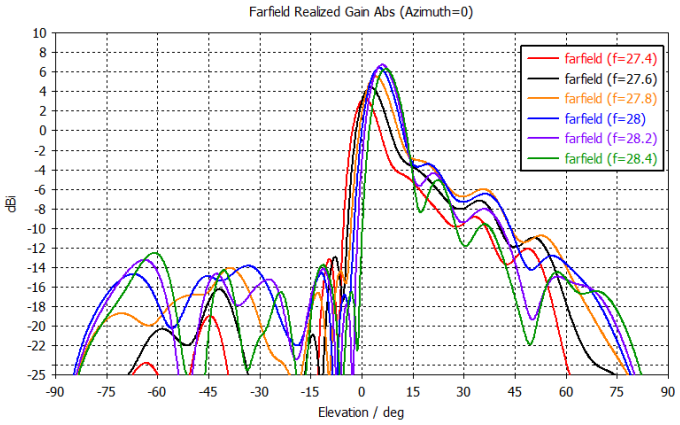

FIGURE 12. Variation of radiation pattern for elevation cut for the optimized simulation over frequency.

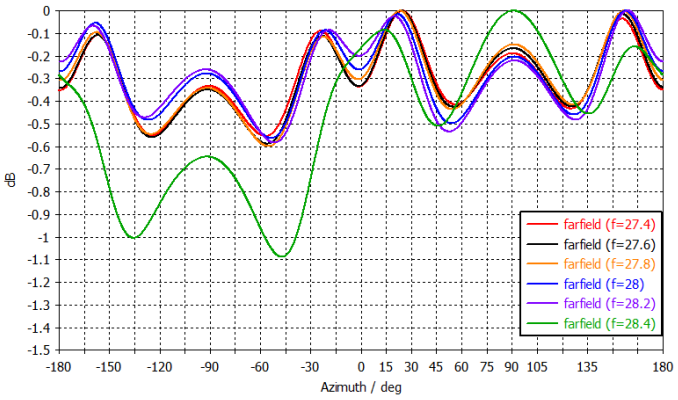

FIGURE 13. Variation of radiation pattern for azimuth cut for the optimized simulation over frequency.

4.4. SIW Transition and Characterization

To allow the construction and tests of the prototype, it is necessary to design a transition from SIW to 50 Ω coplanar with ground transmission line (CPWG). The transition proposed here, based on [19], and also a 50 Ω coaxial connector interface, here a 2.92 mm connector, was designed by adjusting the length and width of the tapered CPWG line to achieve the return loss matching at the simulation in *CST Microwave Studio*. The model of the transition is seen in Fig. 16 with the simulated S parameters response shown in Fig. 15.

After the prototype manufacturing, a SIW with CPWG transition and coaxial connector PCB, with 115 mm of SIW section and 123 mm in total length and seen in Fig. 17, was also produced and characterized in a network analyzer and the return loss results presented concordance with the simulation, but higher insertion losses were noticed, as seen in Fig. 18. This loss is commonly associated with the electroless nickel immersion gold (ENIG) PCB finish and the copper roughness [20], which has a significant impact on mm-wave frequencies due to the skin-depth effect, and dielectric loss variations. Based on these measurements, a complete simulation model with reduced metal conductivity, to represent the increase of losses due to the addition of ENIG finishing and the equivalent conductivity reduction with the surface roughness, was created to compare the simulated and measured results. All the results are available in Fig. 18.

4.5. Connectorized Antenna Model

With the results of the previous section, two simulation models were constructed to analyze the impacts of the insertion of the SIW to CPWG and the coaxial connector in the antenna, the complete simulation model and the complete simulation with loss correction model, with the last one using the reduced conductivity for the metal layers obtained in the previous section.

TABLE 1. Parameters of slots before and after the optimization.

Slot	Position (mm)	Admitance (mS)	Offset (mm)	Length (mm)	Optim. Adjust	Optimized Length (mm)
1	0,00	0,022	−0, 017	3,998	0,9478	3,789
2	9,64	0,034	−0, 019	4,079	0,9662	3,941
3	14,82	0,027	0,018	3,931	-	3,931
4	19,61	0,033	−0, 019	3,941	-	3,941
5	24,89	0,106	0,026	4,004	-	4,004
6	30,33	0,041	−0, 020	3,939	-	3,939
7	34,90	0,210	0,036	4,017	-	4,017
8	40,92	0,206	−0, 036	3,979	0,9820	3,907
9	44,97	0,243	0,039	4,001	0,9612	3,845
10	51,18	1,677	−0, 090	4,195	0,9959	4,178
11	57,60	1,664	0,090	4,187	0,9960	4,171
12	63,66	0,236	−0, 038	3,998	0,9747	3,897
13	67,84	0,217	0,037	3,982	0.9815	3,908
14	73,73	0,196	−0, 034	4,012	-	4,012
15	78,39	0,050	0,021	3,940	-	3,940
16	83,73	0,093	−0, 025	3,991	-	3,991
17	88,93	0,041	0,020	3,944	-	3,944
18	93,81	0,022	−0, 018	3,927	-	3,927
19	98,88	0,038	0,019	4,080	0,9590	3,913
20	108,57	0,023	0,018	3,999	0,9616	3,845

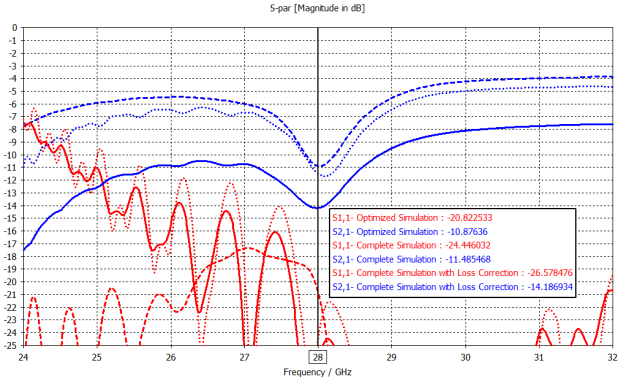

FIGURE 14. Comparison among S parameters for the Optimized, Complete, and Complete with loss correction models.

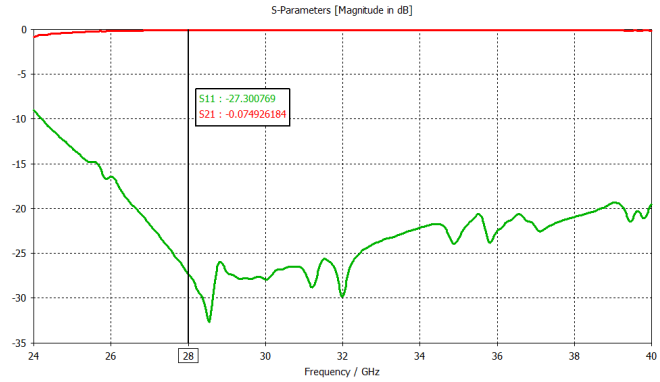

FIGURE 15. Simulated S parameters result for the SIW to CPWG and coaxial transition from Fig. 16.

The addition of the transition and coaxial connectors impacted the radiation pattern results for some higher elevations, as seen in Fig. 19 comparing all three simulation results, and the reduction of the gain is noticeable for the model with loss correction and the same results for the normalized elevation cut seen in Fig. 20. The analyses of both, the gain and the normalized radiation pattern pattern, are important here to see the impact of the SIW in the shape of the beamform synthesis beyond the reduction of the gain, once the increase of losses along the SIW reduces the amplitude of the slots proportionally to the slot position, changing the amplitude calculated for each array element. Analyzing these results, it is possible to see a small variation, around 1 dB, of the normalized radiation pattern in the synthesized region, from 0° to 60° and from 120° to 180°, caused by the increase of losses impact. Also, the variation is caused by the coaxial connector, once the comparison of the results with the optimized model in the front of the antenna (0°–60°) shows a major deviation compared to the back of the antenna (120°–180°), where the connector volume is significantly smaller.

Furthermore, the transition and connector addition causes a variation in the ripple analysis of the normalized omnidirectional pattern azimuth cut in Fig. 21 going from 0.6 dB to 1.8 dB, with no significant impact regarding the increase of in-

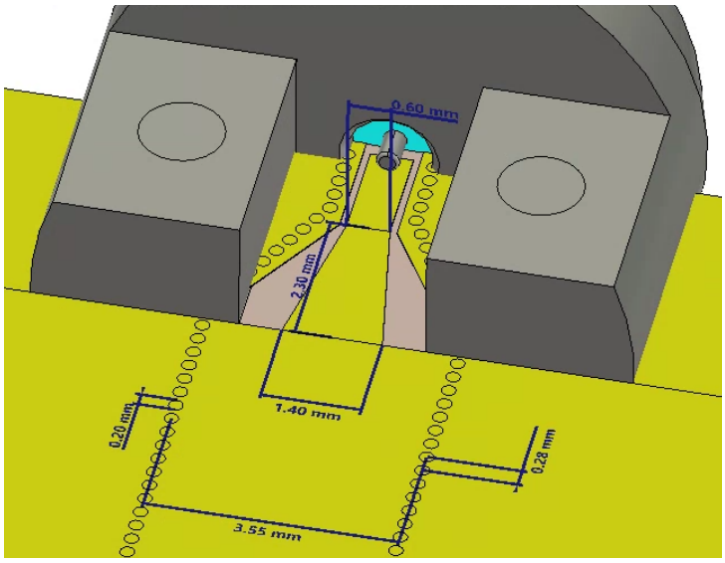

FIGURE 16. Dimensions of the SIW, the SIW to CPGW transition, and the 2.92 mm connector.

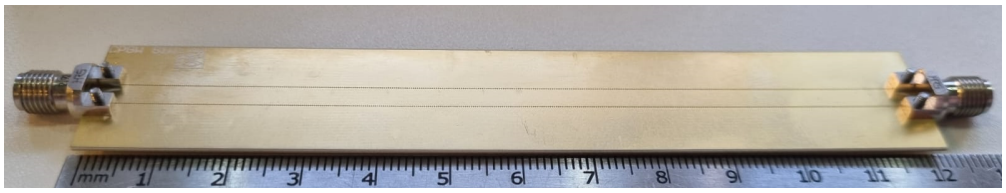

FIGURE 17. SIW with CPWG transition PCB and connectors manufactured.

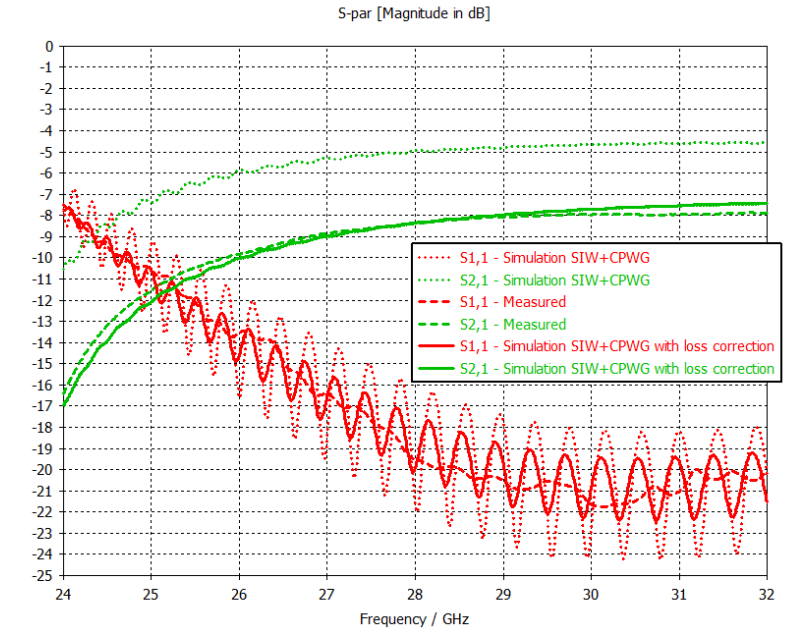

FIGURE 18. Comparison between measured, 3D simulation results with and without loss correction for a 123 mm PCB with coaxial connectors, CPWG transitions, and a SIW section of 115 mm.

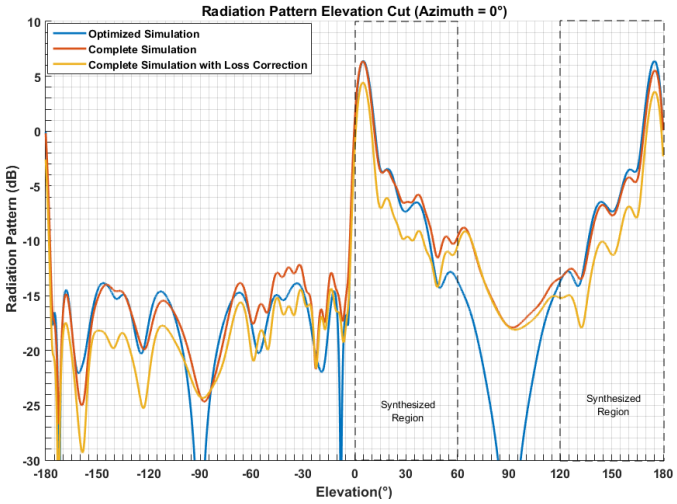

FIGURE 19. Comparison among radiation patterns at elevation cut for the Optimized, Complete, and Complete with Loss Correction models simulation results.

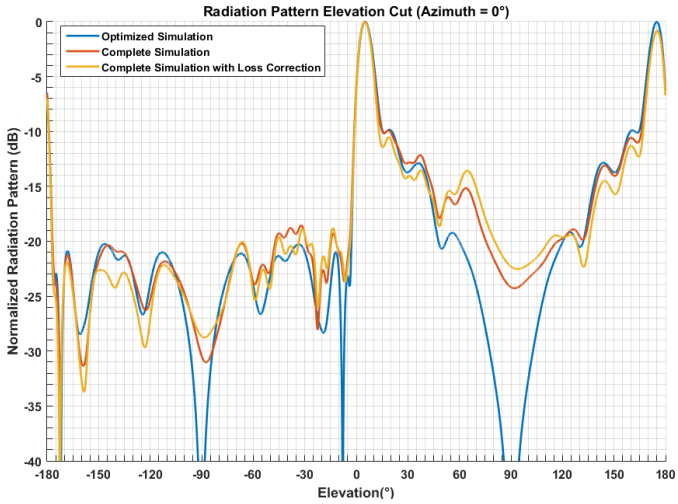

FIGURE 20. Comparison among normalized radiation patterns at elevation cut for the Optimized, Complete, and Complete with Loss Correction models simulation results.

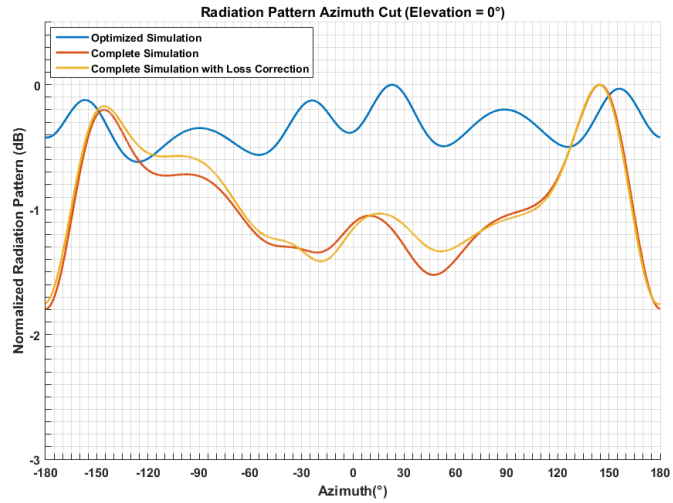

FIGURE 21. Comparison between the simulated results (optimized and complete) for Azimuth cut.

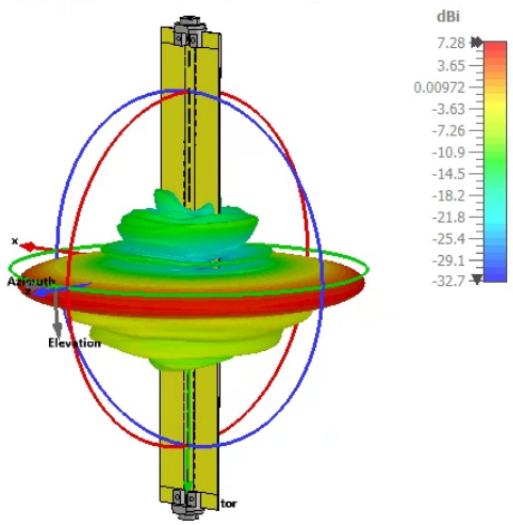

FIGURE 22. 3D simulated radiation pattern for the complete model.

sertion loss, comparing the model with and without loss correction. Here, the normalized radiation pattern is important to analyze the variation caused by the connector insertion on the omnidirectionality of the antenna.

The 3D simulated radiation pattern and model are shown in Fig. 22. The complete simulation found that efficiency due to losses in the load termination, defined as the ratio between the radiated power and the sum of the radiated power and the load termination power, was 84.5% for the complete model and 85.1% for the model with loss correction.

The simulated maximum gain is 7.3 dB for the complete model (Fig. 22) and 5.2 dB for the complete model with loss correction. The simulated gain for the 0° azimuth cut is 6.4 dB for the complete model and 4.4 dB for the model with loss correction (Fig. 19). The difference of 2 dB between the models is similar in both cases.

Comparing the results, the increase of the maximum gain of the model without loss correction is noticeable in comparison to the optimized model (from 6.8 to 7.3 dB, comparison of maximum in Fig. 22 and Fig. 11). It occurs due to interference of the connector addition, due to constructive and destructive interferences, once it increases the radiation pattern variation at azimuth cut (from 0.6 to 1.8 dB in Fig. 21) and also increases the difference between the maximum gain and the 0° azimuth cut gain. Adding these variations to the radiation pattern, part of the gain will be higher, such as the maximum gain, and part will be lower, as the back region maximum of the complete simulation at the elevation cut in Fig. 19.

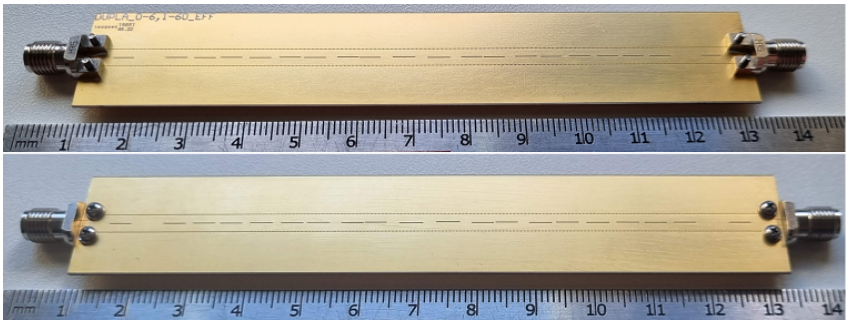

FIGURE 23. Antenna prototype, top and bottom.

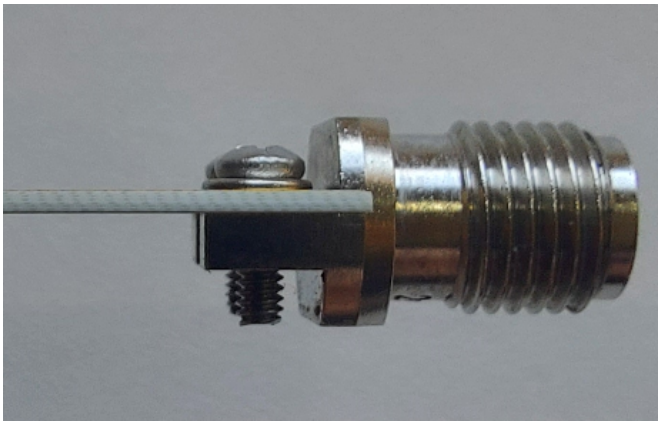

FIGURE 24. Side view of prototype, showing the two layers and dielectric substrate.

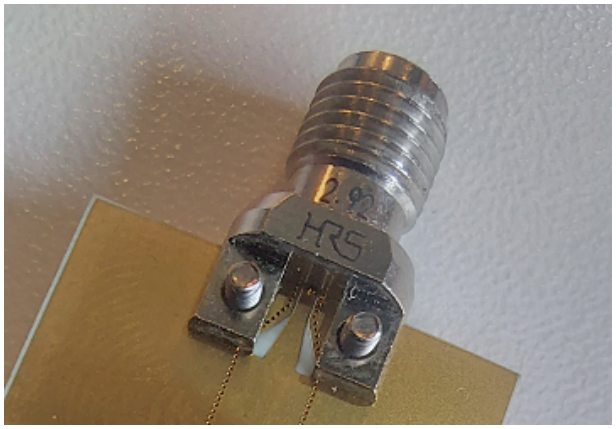

FIGURE 25. SIW to CPWG and coaxial connector transitions.

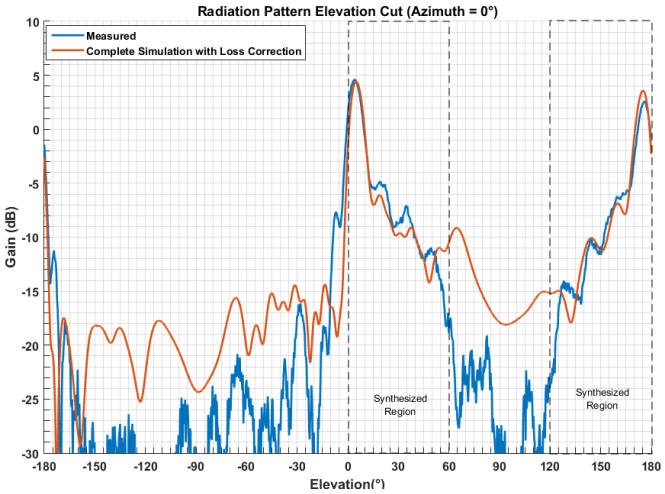

FIGURE 26. Comparison between the measured and simulated results for elevation cut.

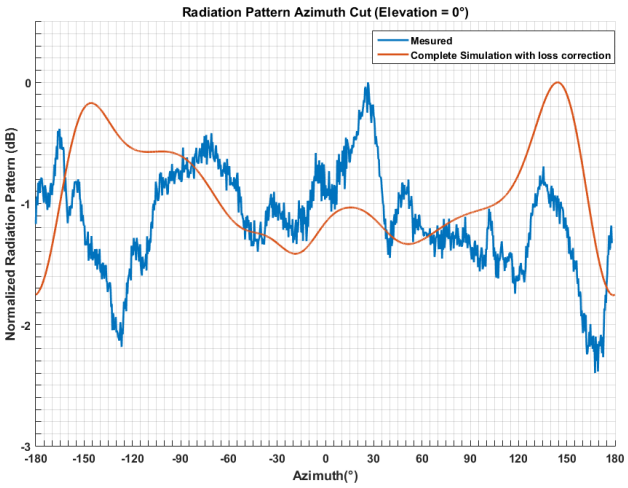

FIGURE 27. Comparison between the measured and simulated results for azimuth cut.

Based on the efficiency presented here resulting from power dissipated in the load, the loss is estimated to be approximately 0.8 dB when comparing only the load and radiated power. In the overall model, which accounts for power and losses in all materials, the loss from load dissipation is smaller than the dielectric and conductor losses, even in models that do not include conductivity loss corrections.

5. MEASUREMENT AND RESULTS

The prototype, shown in Fig. 23 with side view in Fig. 24 and SIW to CPWG and coaxial connector transitions detailed in Fig. 25, was characterized in S parameters and anechoic chamber for radiation pattern measurements.

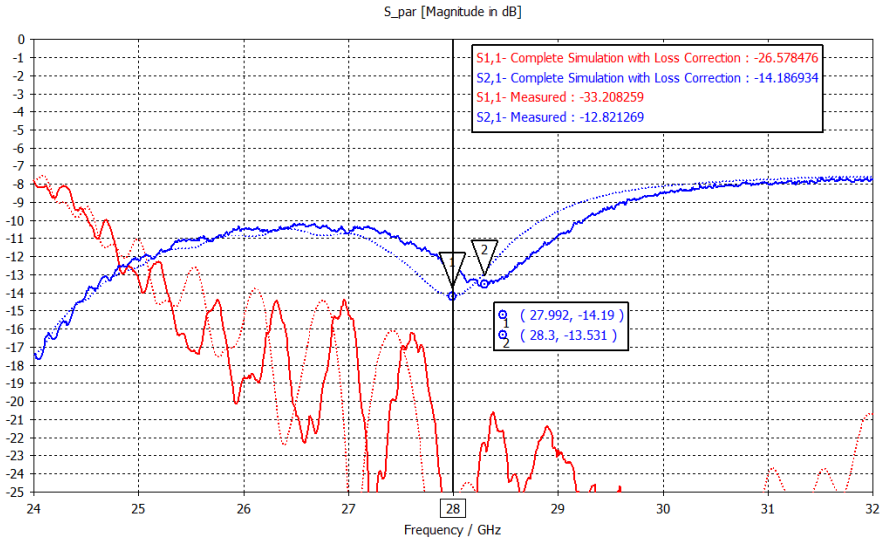

FIGURE 28. Comparison between the measured and simulated results of S parameters.

A high coherence between simulation and measurement can be observed for the elevation cut in Fig. 26, especially in the synthesized $\csc^2$ region, which goes from 0 to 60° and 120 to 180° due to the omnidirectional azimuth radiation pattern. The difference around 60° observed in the graphic, but not observed around 120° is caused by the connector, as demonstrated by Fig. 10, and the measure is more similar to the optimized simulation in that part. The fixing bracket used during the elevation cut measurement can explain this difference, reducing the impact of the connector, which also impacts the measured results around +90° and −90°. The sidelobes were optimized to be under 20 dB, confirmed by measurement.

In the azimuth omnidirectional radiation pattern shown in Fig. 27, a ripple of 2.4 dB is observed in the measurement and 1.8 dB in the simulation. The impact of the connector on the simulation result is evident compared to the ripple of the simulated model without the connector, which was 0.6 dB.

The S parameter results in Fig. 28 show a small deviation of 1% compared with the simulated results, but without major impacts on the radiation pattern synthesis, as it is possible to notice in the measurement results. Usually, this variation can be explained by the increase of conductor thickness due to ENIG PCB finish, which can shift the resonance frequency of the slot, the variation of the dielectric constant of the PCB, or deviations between the connector modeling and mounting.

6. CONCLUSION

The proposed antenna was designed, prototyped, and characterized. The results were coherent with the simulations and established requirements. A slight deviation of 1% in the S parameters results was observed; however, this did not affect the main requirements: the synthesis of the $\csc^2$ radiation pattern at the elevation plane and the omnidirectional radiation at the azimuth plane.

The radiation pattern was verified through tests conducted in an anechoic chamber, presenting a slight variation for the azimuth cut from 1.8 dB to 2.4 dB. Regarding the elevation cut, the measurement shows a high coherence for the synthesized region from 0° to 60° and from 120° to 180°, with a reduction of the expected impact of the insertion of the connector around 60°, making the results agree more with the optimized results without it. The mounting of the antenna in fixing brackets and cable to enable elevation cut characterization can explain this variation, which also accounts for the variation in side lobes around +90° and −90°. The side lobes outside the synthesized region were optimized to be below 20 dB, a goal that was achieved.

All the intermediate results and steps were demonstrated, including the impact of connectors and transitions and the description of the development process, which can be used to develop antennas with different radiation patterns for various applications for different coverage areas, with the possibility of adding nulls to the desired radiation pattern to avoid obstacles.

The synthesis methodology proposed for the $\csc^2$ radiation pattern showed its robustness even with the higher losses discussed, which could have a higher impact on the final radiation pattern. The losses due to the power dissipated in the load, another point of discussion for this project, were lower than the losses in the materials for the simulated models.

As discussed, higher losses were observed at measurements than the original simulation, attributed to ENIG PCB finish and copper roughness. Different PCB finishes can be applied to solve this issue, such as electroless nickel electroless palladium immersion gold (ENEPIG), hard gold, bared copper, or other nickel-less options, and a lower-roughness copper process. Also, lower-loss substrates, such as teflon-based types, can be employed to reduce dielectric losses.

The antenna is cost-effective due to its design as a two-layer PCB without blind or buried vias and no machined components. The use of blind and buried, besides cost impacts the integration between the antenna and front-end PCB because it depends on the PCB stack-up compatibility. The integration between this

antenna and the front-end circuit PCB is limited only by the relation between the SIW width and the PCB thickness to guarantee the TE_{10} mode propagation on the waveguide.

An important highlight here is that the final model to be integrated with microwave circuit PCBs, one of the advantages of this development, does not need the coaxial connectors, once it is directly integrated into components of the PCB. This makes the model of interest closer to the optimized model, with higher omnidirectionality and higher concordance with the beam-shaped synthesis, as seen in the optimized model and confirmed with the back results (between 120° and 180°) of the connectorized antennas, presenting lower impact of the connector in the elevation radiation pattern.

ACKNOWLEDGEMENT

This work was partially supported by the São Paulo Research Foundation (FAPESP) under the projects 2021/06506–0 (StReAM), 2021/11380–5 (CPTEn), 2021/00199–8 (SMARTNESS), and (EMU) 2022/11596-0; and the Brazilian Agency CNPq, under the project 312714/2019–0 (HEHF's research productivity grant).

REFERENCES

[1] Filgueiras, H. R. D., I. F. d. Costa, A. C. S., J. R. Kelly, and P. Xiao, "A novel approach for designing omnidirectional slotted-waveguide antenna arrays," in *2018 International Conference on Electromagnetics in Advanced Applications (ICEAA)*, 64–67, Cartagena, Colombia, Sep. 2018.

[2] Puskely, J., Y. Aslan, A. Roederer, and A. Yarovoy, "SIW based antenna array with power equalization in elevation plane for 5G base stations," in *12th European Conference on Antennas and Propagation (EuCAP 2018)*, London, UK, Apr. 2018.

[3] Yu, Y., Z. H. Jiang, H. Zhang, Z. Zhang, and W. Hong, "A low-profile beamforming patch array with a cosecant fourth power pattern for millimeter-wave synthetic aperture radar applications," *IEEE Transactions on Antennas and Propagation*, Vol. 68, No. 9, 6486–6496, Sep. 2020.

[4] Kumar, A. and S. Srivastava, "SIW cavity-backed dual inverted L slot antenna array for Ku band applications," *International Journal of Microwave and Wireless Technologies*, Vol. 15, No. 1, 150–155, 2023.

[5] Puskely, J., T. Mikulasek, Y. Aslan, A. Roederer, and A. Yarovoy, "5G SIW-based phased antenna array with cosecant-squared shaped pattern," *IEEE Transactions on Antennas and Propagation*, Vol. 70, No. 1, 250–259, Jan. 2022.

[6] Khodadadi, M., M. Khalily, Z. Davoodirad, A. A. Kishk, and A. Mallahzadeh, "Leaky wave slot array antenna based on gap waveguide technology with cosecant squared pattern for 5G BTS applications," in *2023 IEEE International Symposium On Antennas And Propagation (ISAP)*, 1–2, Kuala Lumpur, Malaysia, Oct. 2023.

[7] Ahmadabadi, H., S. Mallahzadeh, and A. Torabi, "Wide beam reflector antenna with cosecant-squared pattern," *AEU — International Journal of Electronics and Communications*, Vol. 116, 153064, 2020.

[8] Valagiannopoulos, C., "Single-series solution to the radiation of loop antenna in the presence of a conducting sphere," *Progress In Electromagnetics Research*, Vol. 71, 277–294, 2007.

[9] Halder, P., B. Ghosh, S. K. M. Haque, and K. Sarabandi, "Loop antenna over a conducting cone with a spherical cap," *IET Microwaves, Antennas & Propagation*, Vol. 13, No. 14, 2559–2568, 2019.

[10] Gatti, R. V., L. Marcaccioli, and R. Sorrentino, "Design of slotted waveguide arrays with arbitrary complex slot voltage distribution," in *IEEE Antennas and Propagation Society Symposium, 2004*, Vol. 3, 3265–3268, Monterey, CA, USA, Jun. 2004.

[11] Picazo, J. J. G., M. Calvo, J. L. Besada, and J. N. Sahalos, "On the design of nonuniformly spaced slot arrays," *IEEE Transactions on Antennas and Propagation*, Vol. 38, No. 11, 1780–1783, Nov. 1990.

[12] Pasetto, T. P. and H. E. Hernández-Figueroa, "Design of a slotted siw antenna with omnidirectional azimuth pattern and cosecant squared elevation pattern," in *2024 IEEE Texas Symposium on Wireless and Microwave Circuits and Systems (WMCS)*, 1–5, Waco, TX, USA, Apr. 2024.

[13] Xu, F. and K. Wu, "Guided-wave and leakage characteristics of substrate integrated waveguide," *IEEE Transactions on Microwave Theory and Techniques*, Vol. 53, No. 1, 66–73, Jan. 2005.

[14] Gilbert, R. A., *Antenna Engineering Handbook*, McGraw-Hill, 2007.

[15] Enjiu, R. K. and M. B. Perotoni, "Slotted waveguide antenna design using 3D EM simulation," *Microwave Journal*, Vol. 56, No. 7, 72, 2013.

[16] Balanis, C. A., *Antenna Theory: Analysis and Design*, John Wiley & Sons, 2015.

[17] Pozar, D. M., *Microwave Engineering*, John Wiley & Sons, 2012.

[18] Stutzman, W., "Synthesis of shaped-beam radiation patterns using the iterative sampling method," *IEEE Transactions on Antennas and Propagation*, Vol. 19, No. 1, 36–41, Jan. 1971.

[19] Kordiboroujeni, Z. and J. Bornemann, "New wideband transition from microstrip line to substrate integrated waveguide," *IEEE Transactions on Microwave Theory and Techniques*, Vol. 62, No. 12, 2983–2989, Dec. 2014.

[20] Ippich, A., "PCB surface finish impact to losses at high frequencies," in *2019 IEEE International Conference on Microwaves, Antennas, Communications and Electronic Systems (COMCAS)*, 1–4, Tel-Aviv, Israel, Nov. 2019.